Electronic Supporting Information

All-catecholate-stabilized black titanium-oxo clusters for efficient photothermal conversion

Jinle Hou,*‡[a] Nahui Huang,‡[a], Dinesh Acharya,[b] Yuxin Liu,[a] Jiaying Zhu,[a] Jiaxin Teng,[a] Zhi Wang,[b] Konggang Qu,[a] Xianxi Zhang*[a] and Di Sun*[b]

[a] Shandong Provincial Key Laboratory of Chemical Energy Storage and Novel Cell Technology, and School of Chemistry and Chemical Engineering, Liaocheng University, Liaocheng, 252000, People's Republic of China. E-mail: houjinle@lcu.edu.cn (J. L. Hou); zhangxianxi@lcu.edu.cn (X. X. Zhang).

[b] School of Chemistry and Chemical Engineering, Shandong University, Jinan, 250100, People's Republic of China. E-mail: dsun@sdu.edu.cn (D. Sun).

‡ These authors contributed equally to this work.

Experimental Procedures

Materials and Instruments

Titanium (IV) tetraisopropanolate ($Ti(^iPrO)_4$, 98%, Adamas-beta®), catechol and 3-methylcatechol were purchased from Shanghai Titan Scientific Co., Ltd. Toluene (99.7%), ethylene glycol (99.7%), formic acid (88 %), acetic acid, propionic acid, butyric acid and isopropanol (^iPrOH, 99.7%) were purchased from Sinopharm Chemical Reagent Co., Ltd, China. All chemicals and solvents were analytical grade and used without further purification. Powder X-ray diffraction (PXRD) data were carried out on a microcrystalline powdered sample using a Rigaku SmartLab-9Kw diffractometer using Cu radiation (λ = 1.54184 Å). Thermogravimetry (TG) analysis was performed on a STA449F5/QMS403D instrument (Mettler-Toledo, Schwerzenbach, Switzerland) with a heating rate of 10 °C min^{-1} from 20 to 800 °C in N_2 flow. The solid-state UV/Vis spectra data of the cluster samples were obtained using a Carry 500 UV-VIS spectrophotometer with scanning wavelength range from 200 nm to 900 nm. Fourier transform infrared spectroscopy (FTIR) measurements were obtained using a Nicolet iS50 spectrophotometer. The elemental analyses (C and H) were determined on a Vario EL Cube analyzer. The X-ray photoelectron spectroscopy (XPS) spectra were collected on a Thermo Scientific ESCALAB Xi^+ instrument. The energy dispersive X-ray (EDX) spectra and element mapping of samples were acquired on a Thermo Fisher Scientific FIB-SEM-GX4 scanning electron microscope. Electrospray ionization mass spectra (ESI-MS) of **Ti8** were recorded on a Bruker impact II high definition mass spectrometer, quadrupole and time-of-flight (Q/TOF) modules. The data analysis of the mass spectrum was performed based on the isotope distribution patterns using Compass Data Analysis software (Version 4.4). Electrochemical measurements were carried out on a CHI 660E electrochemical workstation. Photothermal measurements were conducted using CNI Laser MDL-N-450 nm. The photothermal behavior of the sample was monitored by thermal imaging camera (FLIR E54). Infrared photos and real-time temperatures were extracted from the video by FLIR tools software. ^1H NMR spectra of **Ti2** and **Ti16** were recorded on

Bruker-DRX (500 MHz) instruments internally referenced to dimethyl sulfoxide signals.

Synthesis

Synthesis of $Ti_2(Cat)_2(OEgO)_2(OEgOH)_2$ (Ti2)

0.73 mmol (80 mg) of catechol was ultrasonically dissolved in 5 mL of ethylene glycol. 0.33 mmol (0.1 mL) of $Ti(^iPrO)_4$ was added. The mixture was sealed in a 10 mL glass vial and heated at 100 °C for 72 h. After cooling to room temperature, yellow crystals were obtained by filtration and washed several times with ethanol. Yield: 10 mg. Elemental analyses calc. (found) for **Ti2** ($C_{20}H_{26}O_{12}Ti_2$): C, 43.35 (43.56); H, 4.73 (5.17)%.

Synthesis of $Ti_8O_5(Cat)_9(^iPrO)_4(^iPrOH)_2$ (Ti8)

Similar to **Ti2**, except the solvent ethylene glycol was replaced with isopropanol (5 mL). The other conditions were kept the same. After cooling to room temperature, black crystals were obtained by filtration and washed several times with isopropanol. Yield: 60 mg. Elemental analyses calc. (found) for **Ti8** ($C_{72}H_{79}O_{29}Ti_8$): C, 48.28 (48.78); H, 4.45 (4.80)%.

Synthesis of $Ti_{16}O_8(OH)_8(Cat)_{20}\cdot H_2O\cdot PhMe$ (Ti16)

Similar to **Ti2**, except the solvent ethylene glycol was replaced with toluene (5 mL) and formic acid (60 μL). The other conditions were kept the same. After cooling to room temperature, black crystals were obtained by filtration and washed several times with isopropanol. Yield: 30 mg. Elemental analyses calc. (found) for **Ti16** ($C_{134}H_{100}O_{58}Ti_{16}$): C, 47.28 (46.95); H, 2.96 (3.25)%.

Synthesis of $Ti_{16}O_8(OH)_8(MeCat)_{20}\cdot PhMe$ (Ti16-Me)

Similar to **Ti16**, except the catechol was replaced with 3-methyl catechol (0.73 mmol). The other conditions were kept the same. After cooling to room temperature, black crystals were obtained by filtration and washed several times with isopropanol. Yield: 35 mg. Elemental analyses calc. (found) for **Ti16-Me** ($C_{154}H_{136}O_{56}Ti_{16}$): C, 50.07 (49.62); H, 3.76 (4.12) %.

Single-crystal X-ray diffraction

Single crystals of **Ti2**, **Ti8**, **Ti16** and **Ti16-Me** were selected under an optical microscope and rapidly coated with high vacuum grease (Dow Corning Corporation) to prevent decomposition. The single-crystal diffraction analysis of **Ti8** was performed on a Bruker APEX-II CCD diffractometer with graphite-monochromated Mo Kα radiation (λ = 0.71073 Å) at 296 K. In addition, the intensity data and cell parameters of **Ti2**, **Ti16** and **Ti16-Me** were recorded on Bruker D8 VENTURE diffractometer with an Incoatec IμS 3.0 Cu EF (Incoatec IμS diamond Mo) microfocus source (55W, Cu Kα, λ = 1.54184 Å) at 173 K equipped with a PHOTON III C28 detector and an Oxford Cryosystems CryostreamPlus 800 open-fow N_2 cooling device. These structures were solved by the inherent phase method in the SHELXT program and refined by full-matrix least squares techniques against F^2 using the SHELXL program through the OLEX2 interface. Hydrogen atoms at carbon were placed in calculated positions and refined isotropically by using a riding model. Appropriate restraints or constraints were applied to the geometry and the atomic displacement parameters of the atoms in the cluster. All structures were examined using the Addsym subroutine of PLATON to ensure that no additional symmetry could be applied to the models. Pertinent crystallographic data collection and refinement parameters are collated in Table S4. Selected bond lengths are collated in Table S5-S8. The crystallographic data for **Ti2**, **Ti8**, **Ti16**, and **Ti16-Me** were delivered to the Cambridge Crystallographic Data Centre (CCDC) with No. 2294728, 2294731, 2294729, and 2294730, respectively. These data can be obtained from the CCDC via www.ccdc.cam.ac.uk/data_request/cif.

Electrochemical measurements

Photoelectrochemical measurements

Photoelectrochemical measurements were carried out on CHI 660E electrochemical workstation in a standard three-electrode electrochemical cell with a working electrode, a platinum plate as counter electrode and a saturated Ag/AgCl electrode as reference electrode. A sodium sulfate solution (0.2 M) was used as the electrolyte and use a Xe lamp (150 W) was used as the light source. Preparation of the working electrode: 2 mg crystals powder was mixed with 0.99 mL ethanol and 10 μL Nafion D-520 dispersion solutions and sonicated for 30 minutes. Subsequently, 200 μL of slurry was transferred, coated on ITO glass plates (1 cm×2 cm), and then dried at room temperature.

Electrochemical impedance spectroscopy

Electrochemical impedance spectra (EIS) measurements were also carried out on CHI 660E electrochemical workstation via a conventional three-electrode system with a working electrode, a platinum plate as counter electrode and a saturated Ag/AgCl electrode as reference electrode in a 0.2 M Na_2SO_4 aqueous solution over a frequency range of 100 kHz-0.01 Hz.

Computational Studies.

DFT calculations were performed with the Gaussian 16 suite of programs. For the optimizations of the four titanium-oxo clusters (TOCs), **Ti2**, **Ti8**, and **Ti16**, the gradient-corrected B3LYP exchange-correlation functional based on the generalized gradient approximation (GGA) was utilized; LanL2DZ (Los Alamos effective core potential double) basis set was employed for Ti atoms, and 6-31G** basis set was used for C, H, and O atoms. The LANL2DZ basis set containing relativistic effects has been shown to predict accurately Ti nanoclusters' structure-restricted calculations were used for geometry optimization. Harmonic frequencies were then calculated to characterize the stationary points as equilibrium structures with all absolute frequencies and to evaluate zero-point energy (ZPE) corrections. Data for orbital composition analysis with Mulliken partition are from Gaussian 16 calculations and are further processed with Multiwfn and VMD software. The oscillator strength values and weights determined the most probable transitions.

Figure S1. The photos of the crystals of **Ti2**, **Ti8** and **Ti16**.

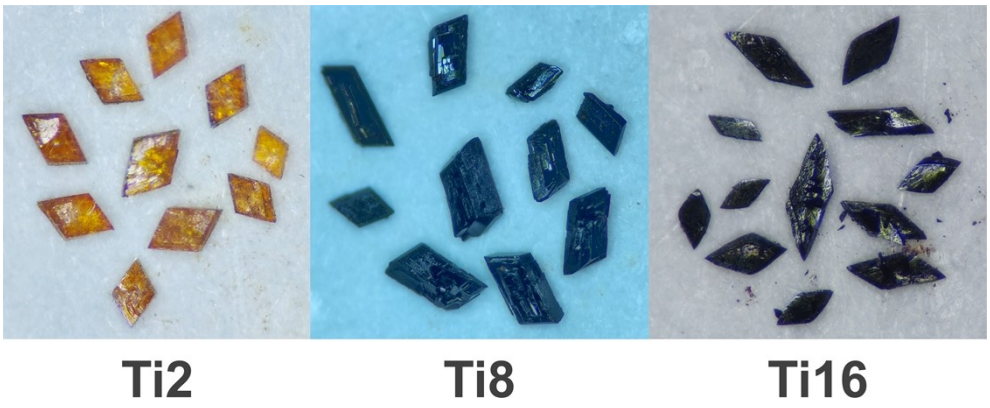

Figure S2. The compared PXRD patterns of **Ti2**.

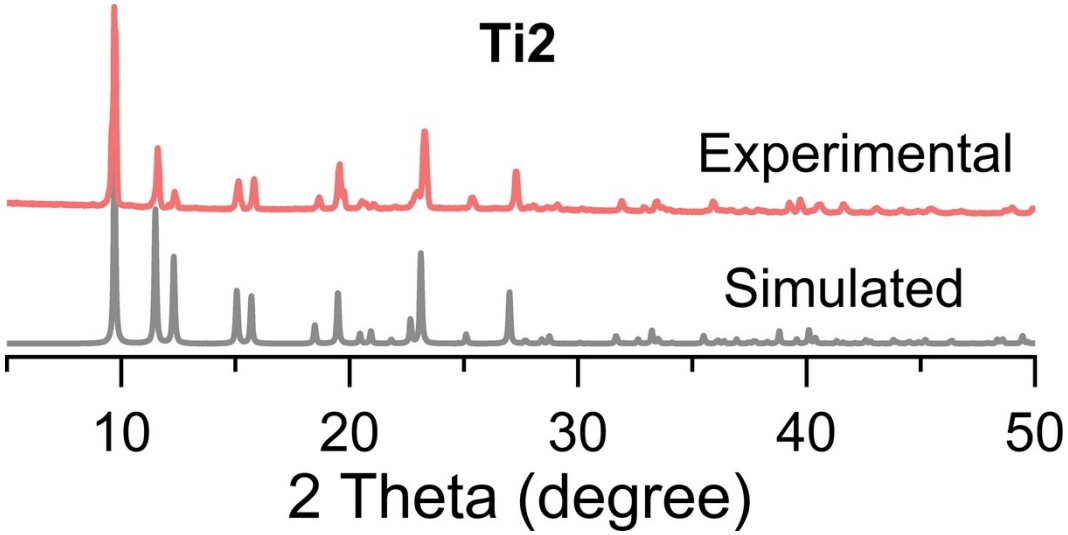

Figure S3. The compared PXRD patterns of **Ti8**.

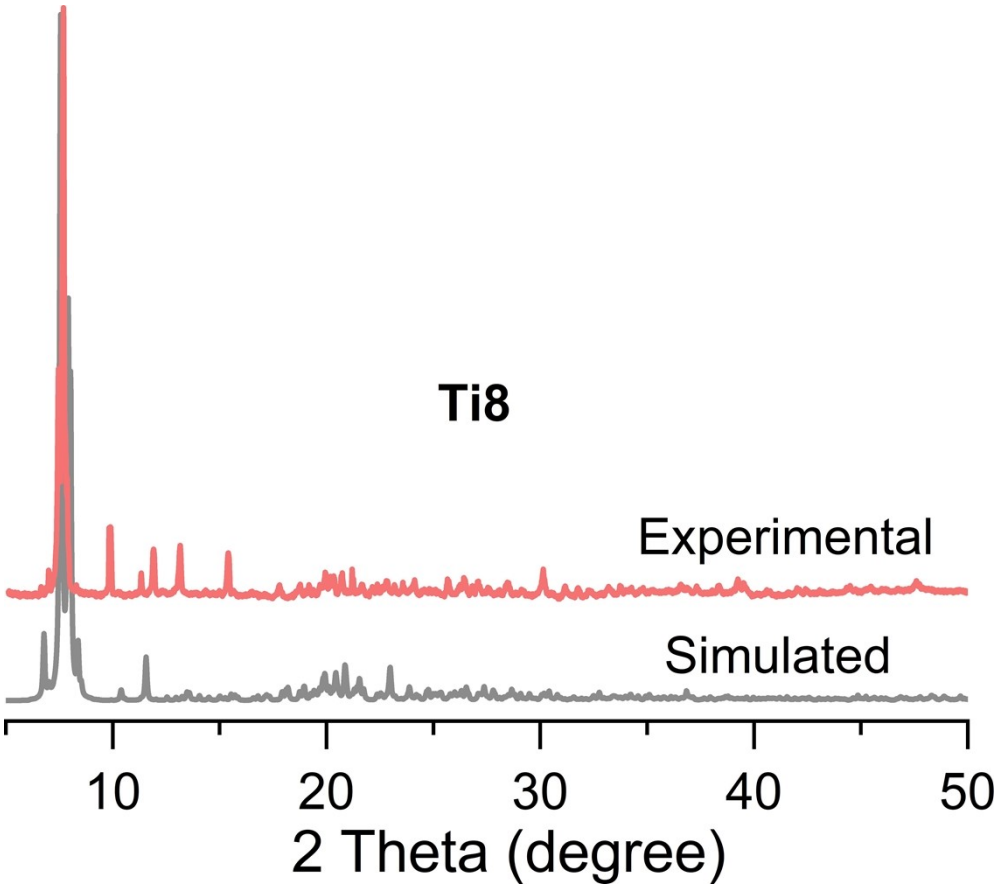

Figure S4. The compared PXRD patterns of **Ti16**.

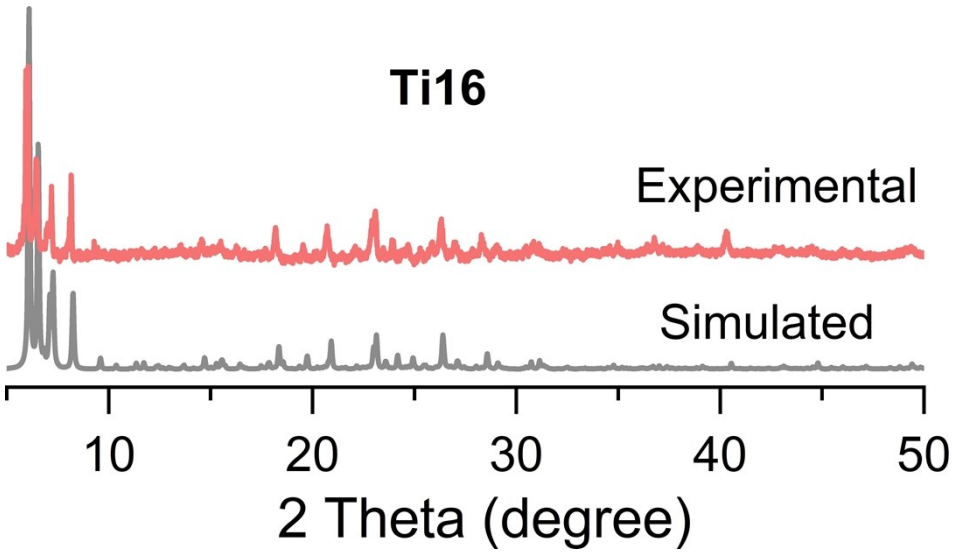

Figure S5. The Fourier transform infrared spectroscopy (FT-IR) of **Ti2**, **Ti8** and **Ti16**.

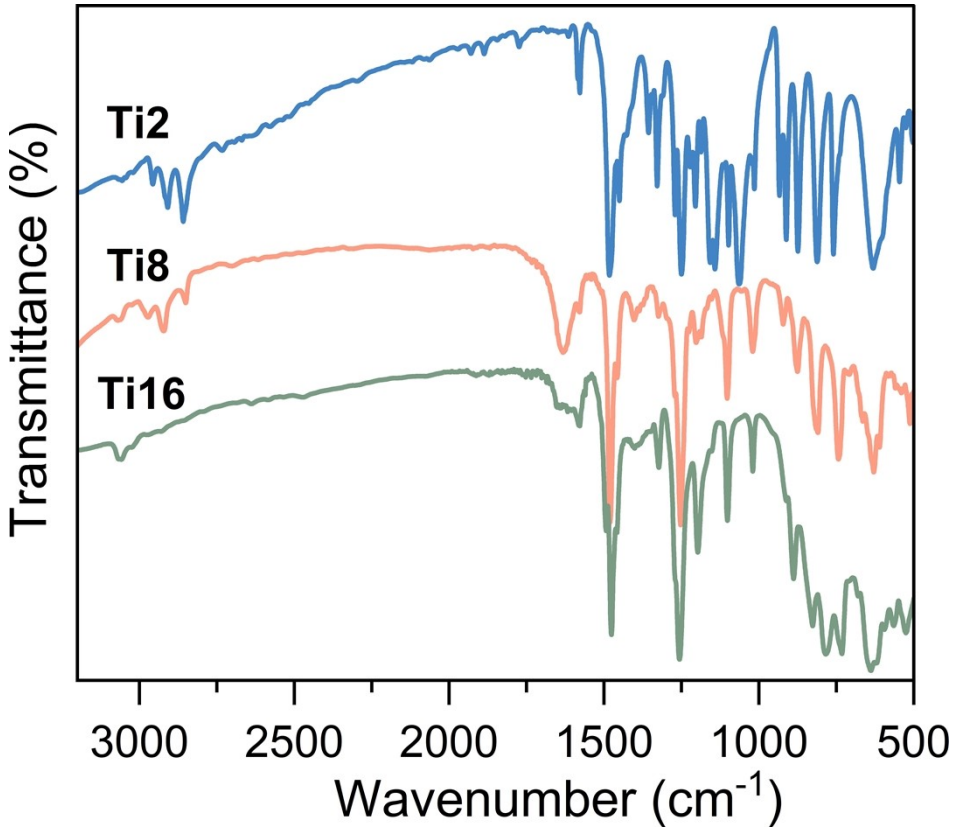

Figure S6. SEM and energy-dispersive X-ray spectroscopy of **Ti2**, **Ti8** and **Ti16**.

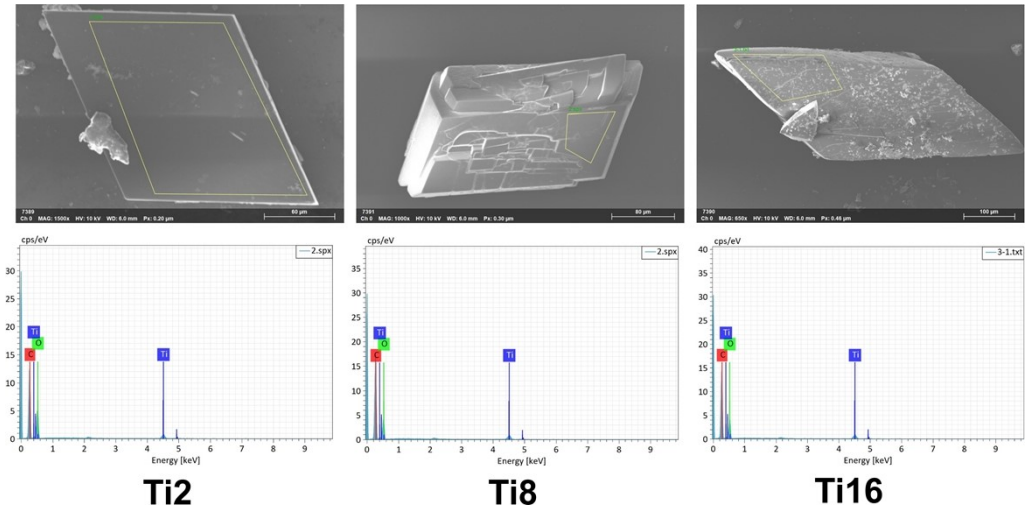

Figure S7. X-ray photoelectron spectroscopy (XPS) spectra of **Ti2**. XPS reveals that all Ti atoms in **Ti2** are exclusively in the +4 oxidization state.

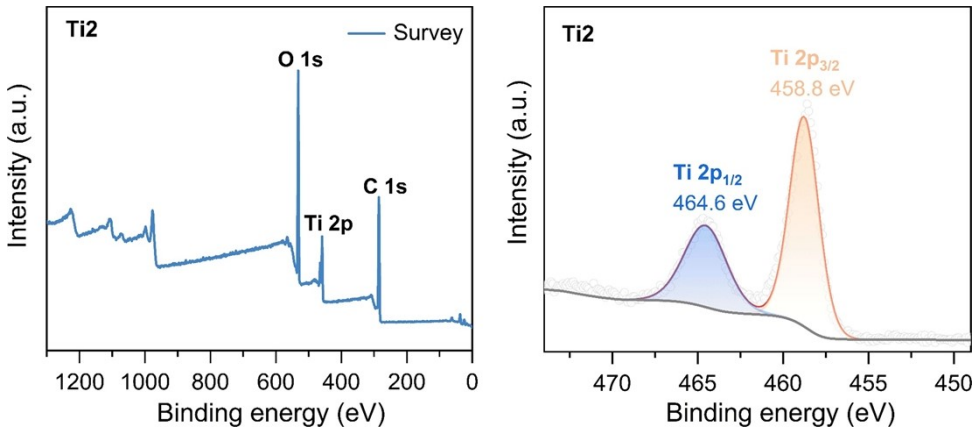

Figure S8. X-ray photoelectron spectroscopy (XPS) spectra of **Ti8**. XPS reveals that all Ti atoms in **Ti8** are exclusively in the +4 oxidization state.

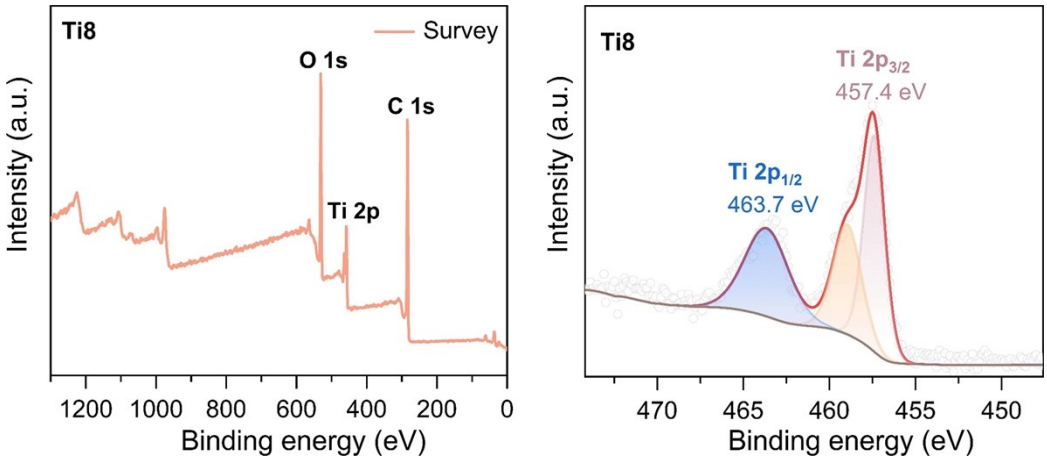

Figure S9. X-ray photoelectron spectroscopy (XPS) spectra of **Ti16**. XPS reveals that all Ti atoms in **Ti16** are exclusively in the +4 oxidization state.

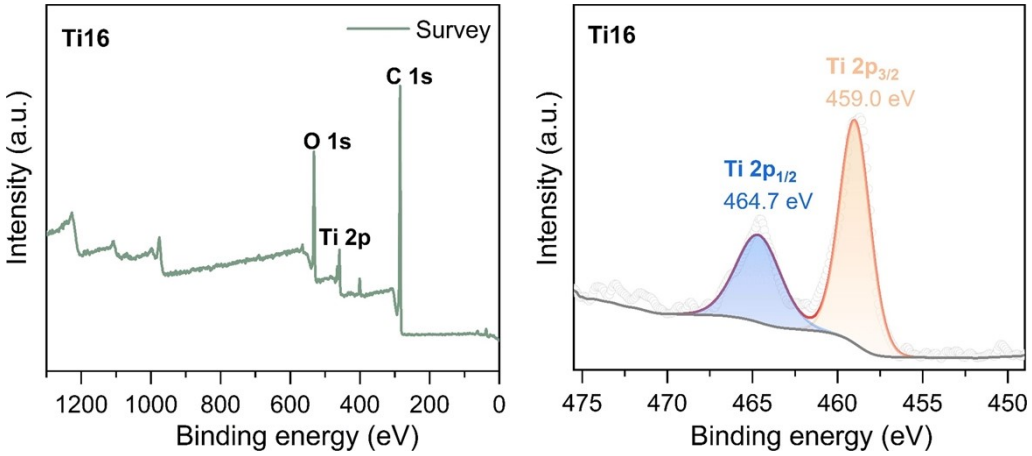

Figure S10. The polyhedral structure of (a) **Ti2**, (b) **Ti8**, and (c) **Ti16**. Green, six-coordinated Ti atom; purple, seven-coordinated Ti atom.

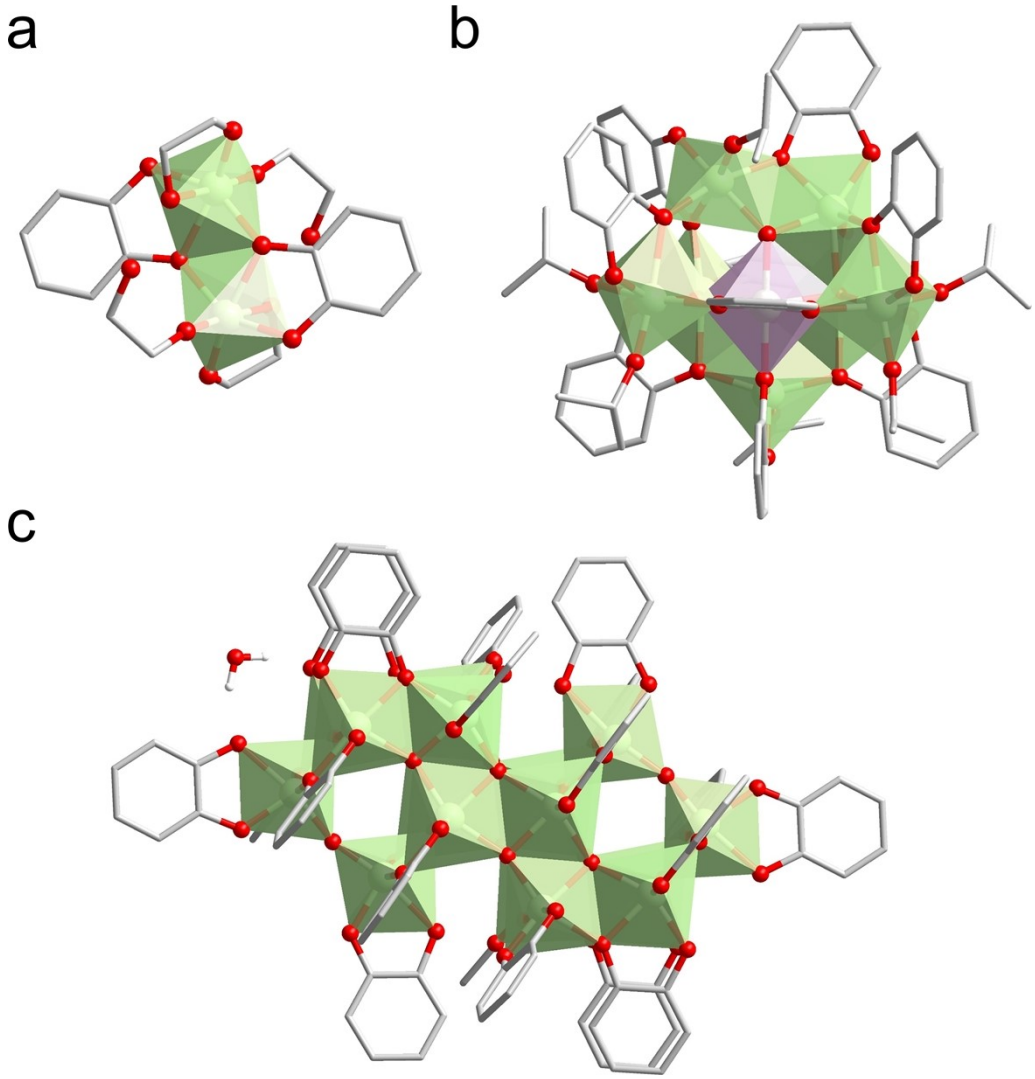

Figure S11. Six pairs of π···π interactions between the phenyl rings and two hydrogen bonding interactions between H_2O and the catechol oxygen atoms of **Ti16**.

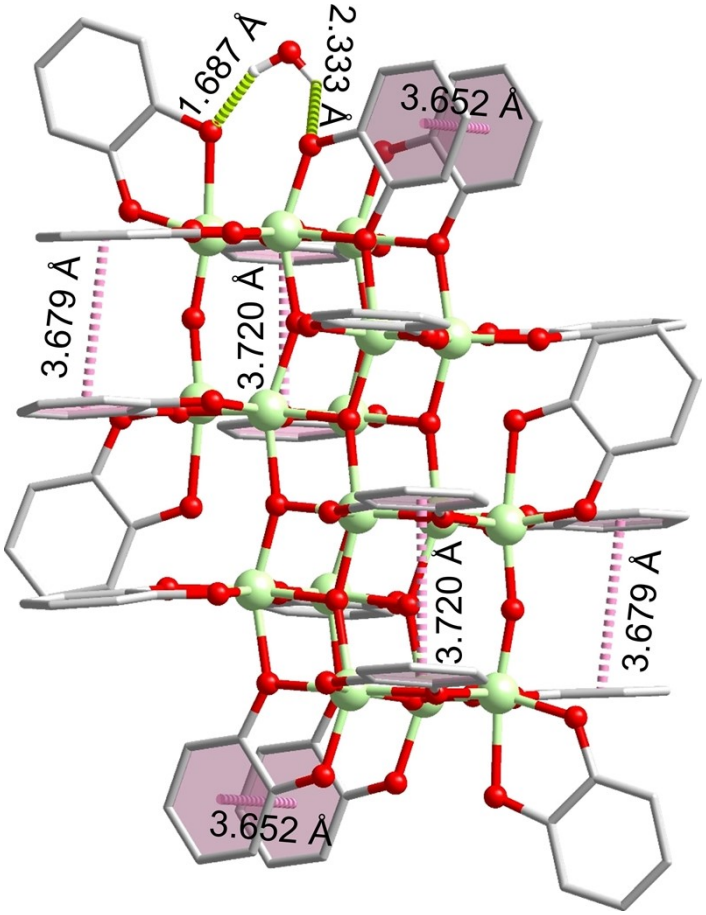

Figure S12. (a) and (b) Overall structure of **Ti16-Me**. (c) The polyhedral structure of **Ti16-Me**.

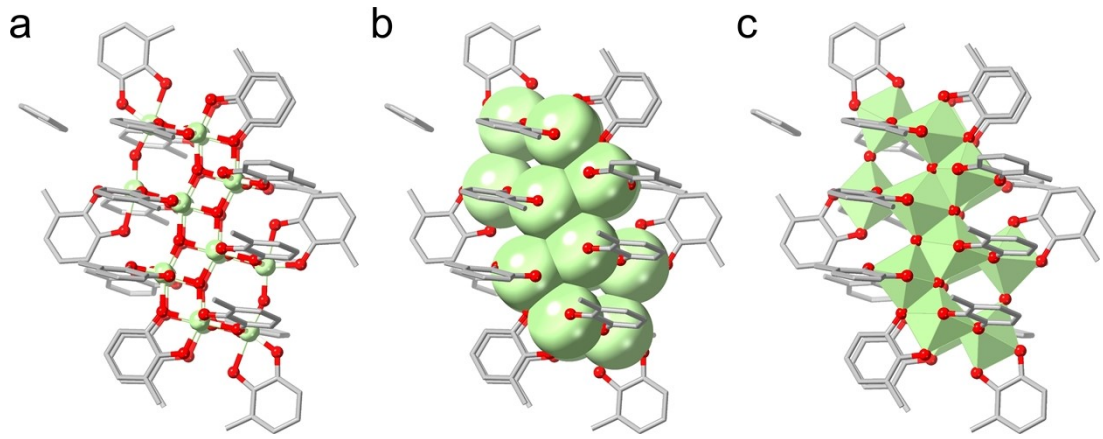

Figure S13. ^{1}H NMR spectrum of **Ti2** in DMSO-d_6.

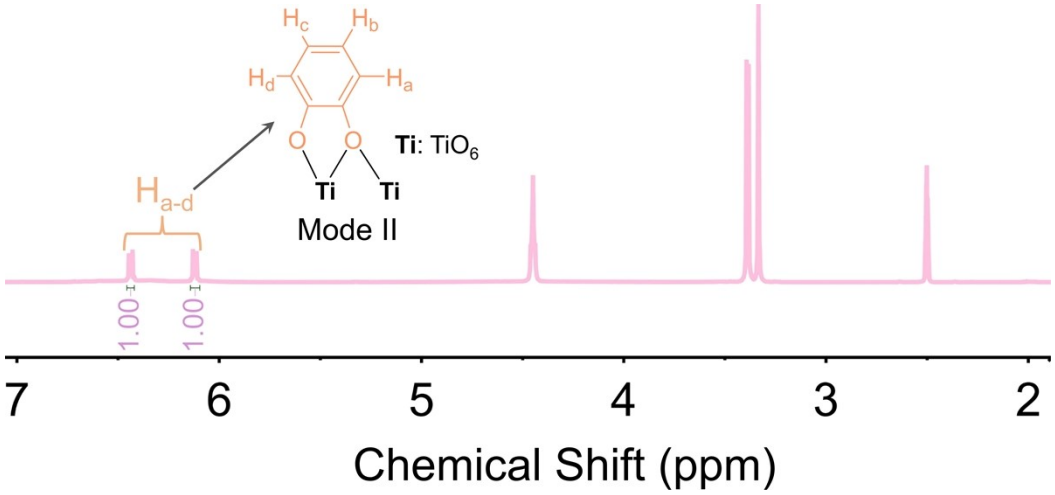

Figure S14. The IR spectras of original crystals and retrieved samples of **Ti16** after soaked in water solutions with pH ranging from 1 to 11 for 48 hours.

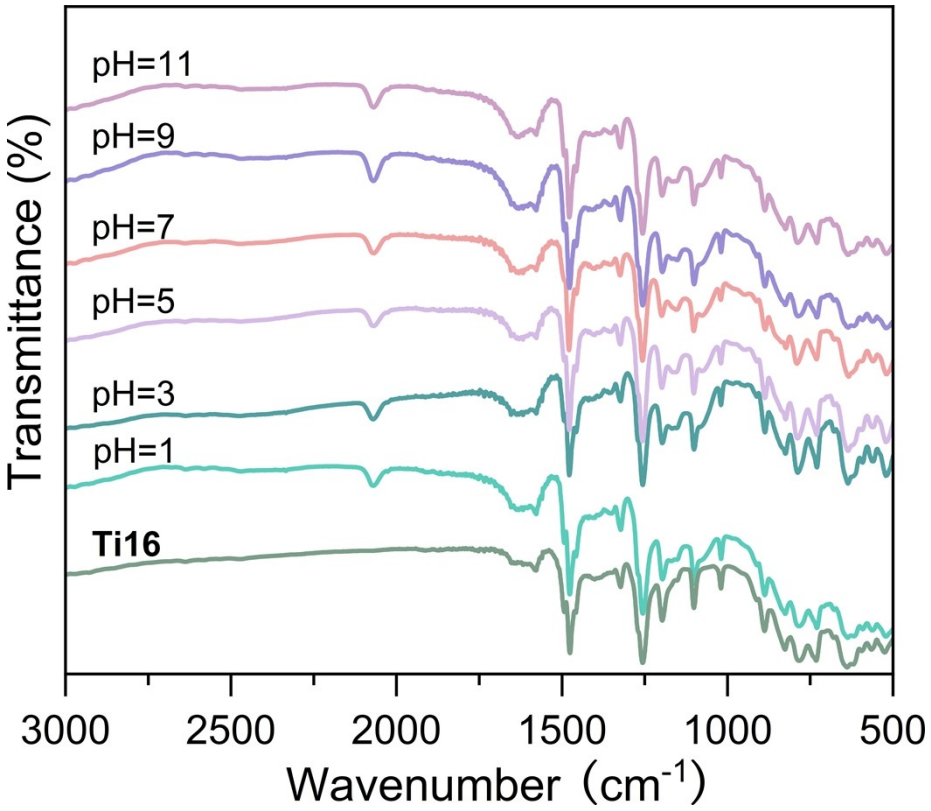

Figure S15. The IR spectras of original crystals and retrieved samples of **Ti16** after soaked in common organic solvents for 48 hours.

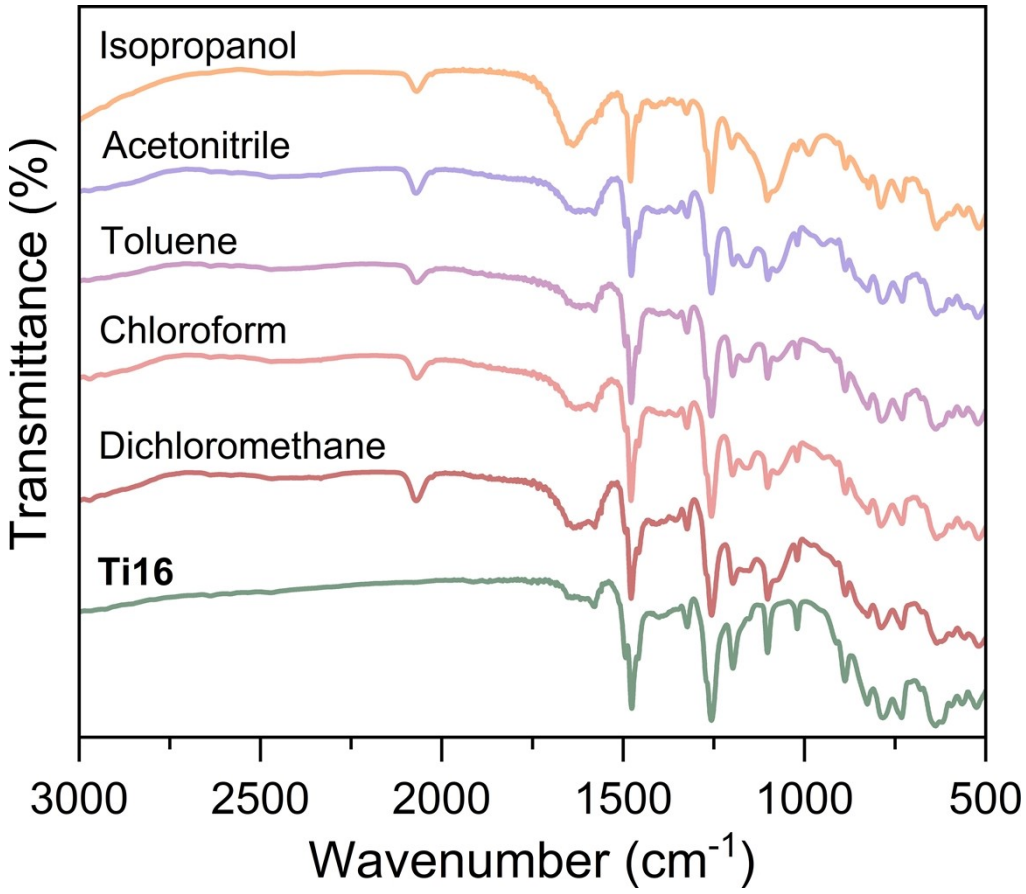

Figure S16. The IR spectras of original crystals and retrieved samples of **Ti8** after soaked in water solutions with pH ranging from 1 to 11 for 48 hours.

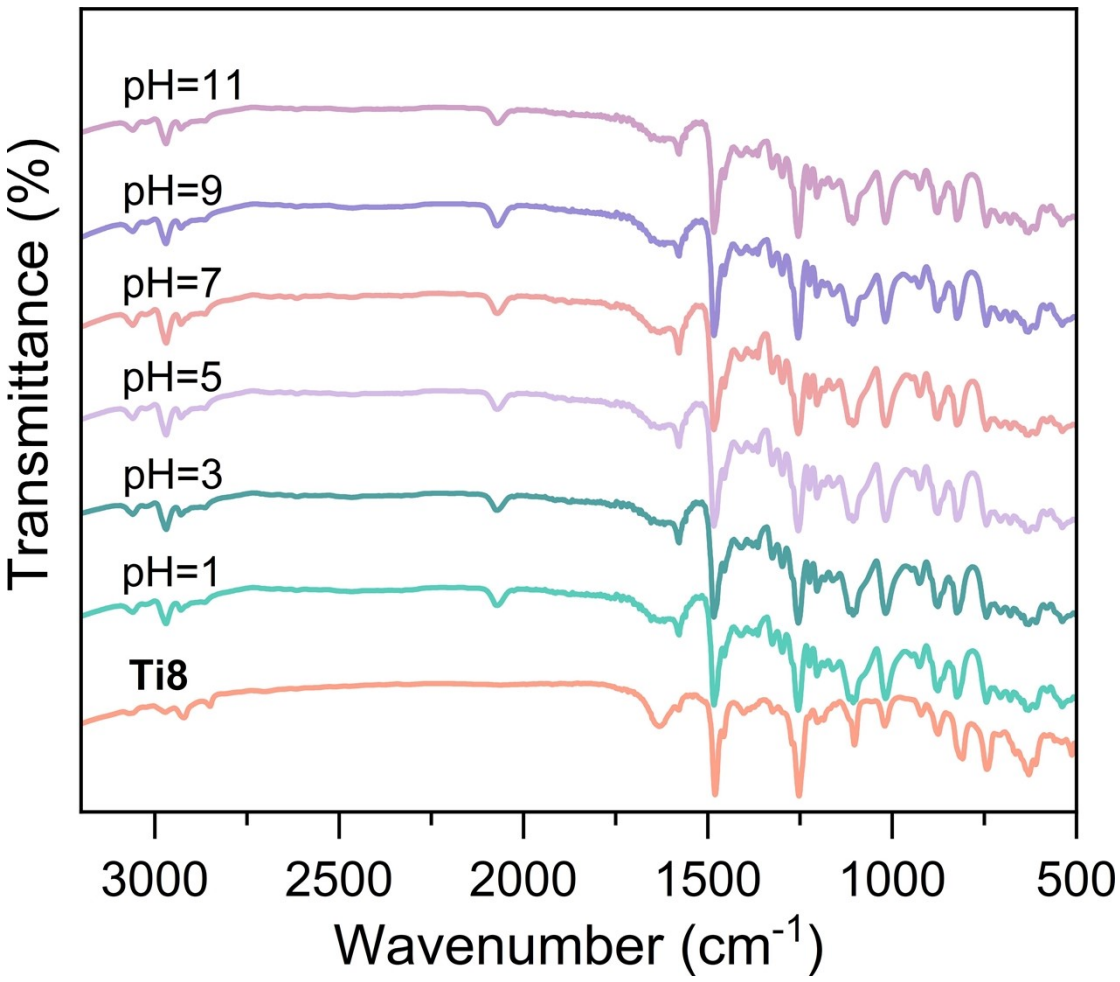

Figure S17. PXRD pattern of **Ti8** soaked in water solutions with pH ranging from 1 to 11 for 48 hours.

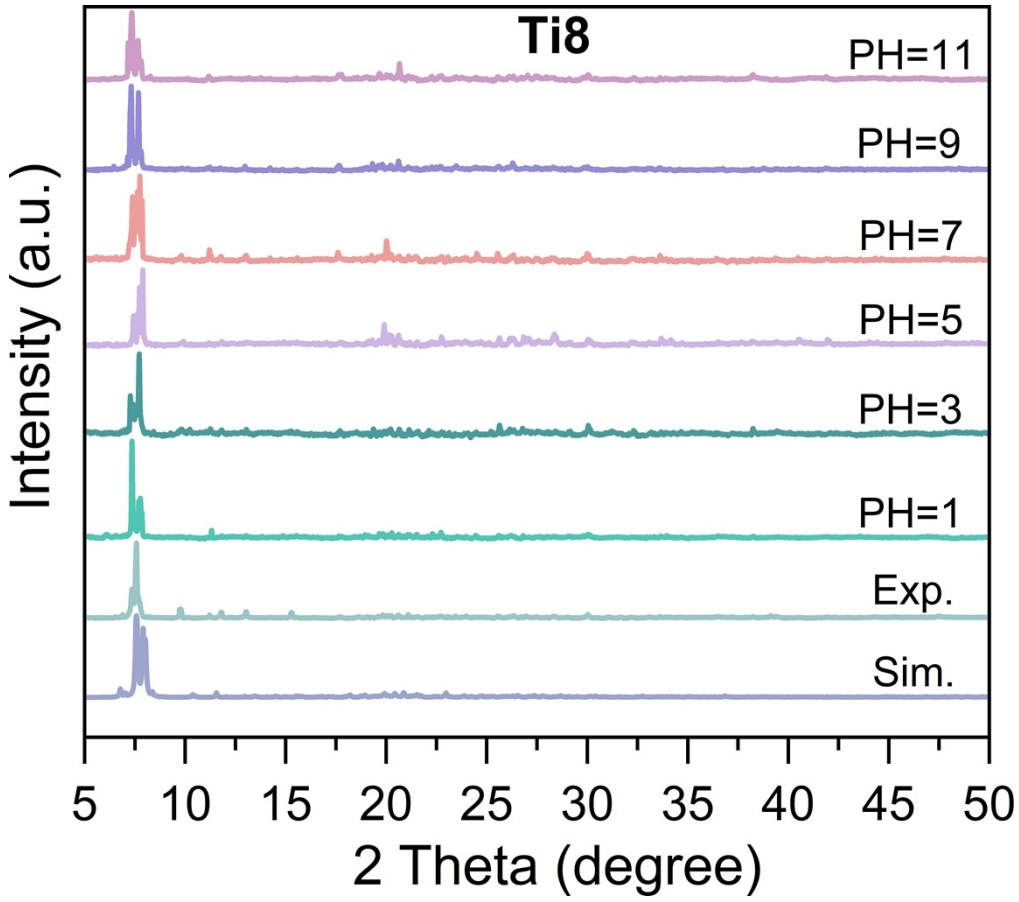

Figure S18. PXRD pattern of **Ti8** under different conditions：exposed to air for one week and soaked in common organic solvents for 48 hours.

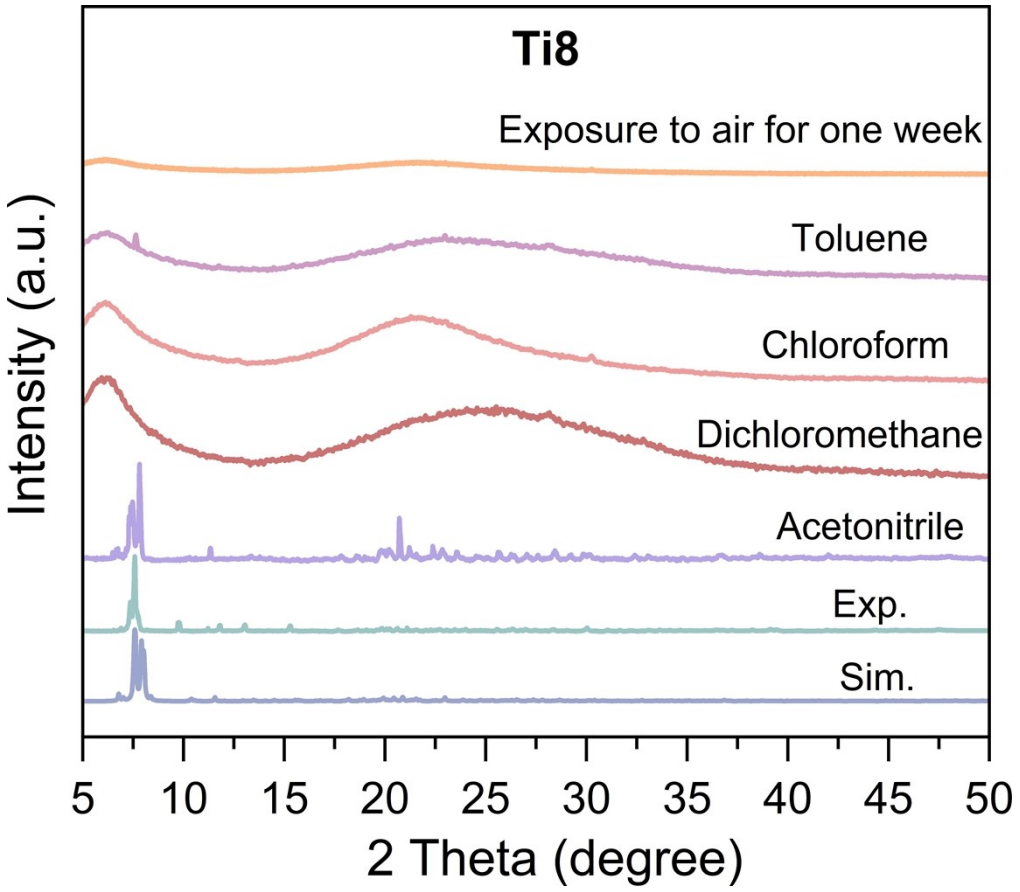

Figure S19. Thermogravimetry analysis (TGA) curve of **Ti2**, **Ti8** and **Ti16**.

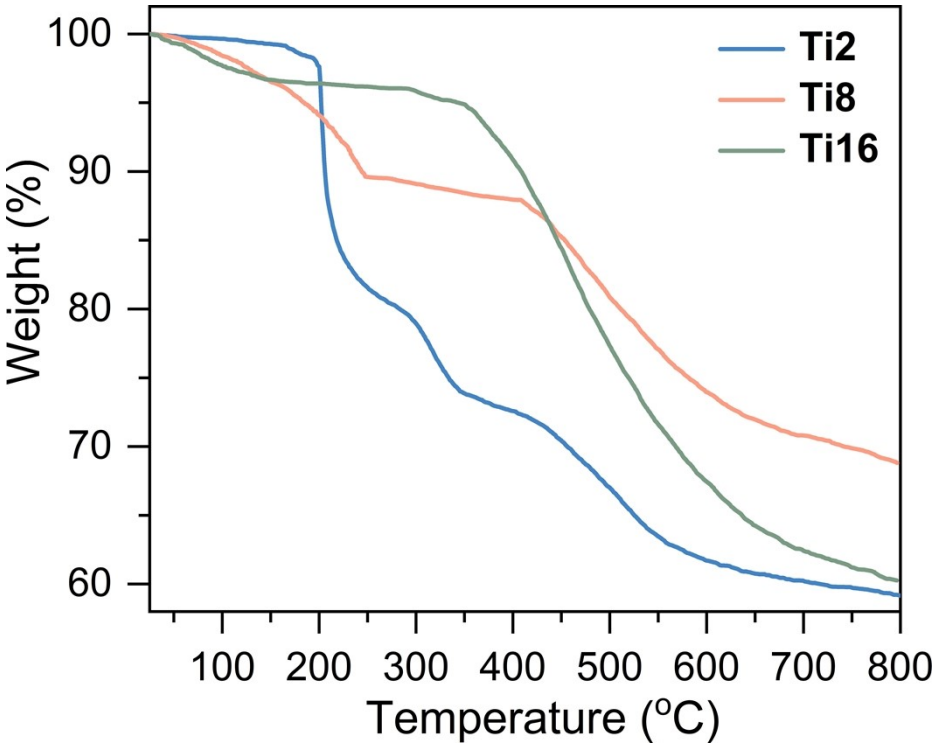

Figure S20. (a) Total structure of the **Ti16**. (b) Total structure of the $Ti_{16}O_{16}(OEt)_{32}$. (c) Total structure of the $Ti_{16}O_{22}(PA)_{20}(O^tBu)_2$. Color code: light green, Ti; red, O; gray, C.

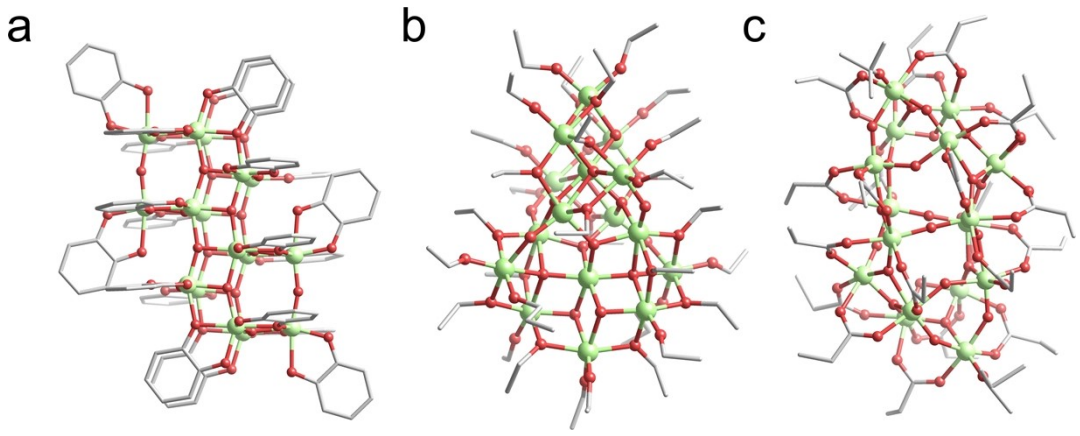

Figure S21. The IR spectra of the original crystals and the samples of **Ti2** after the photoelectrochemical test.

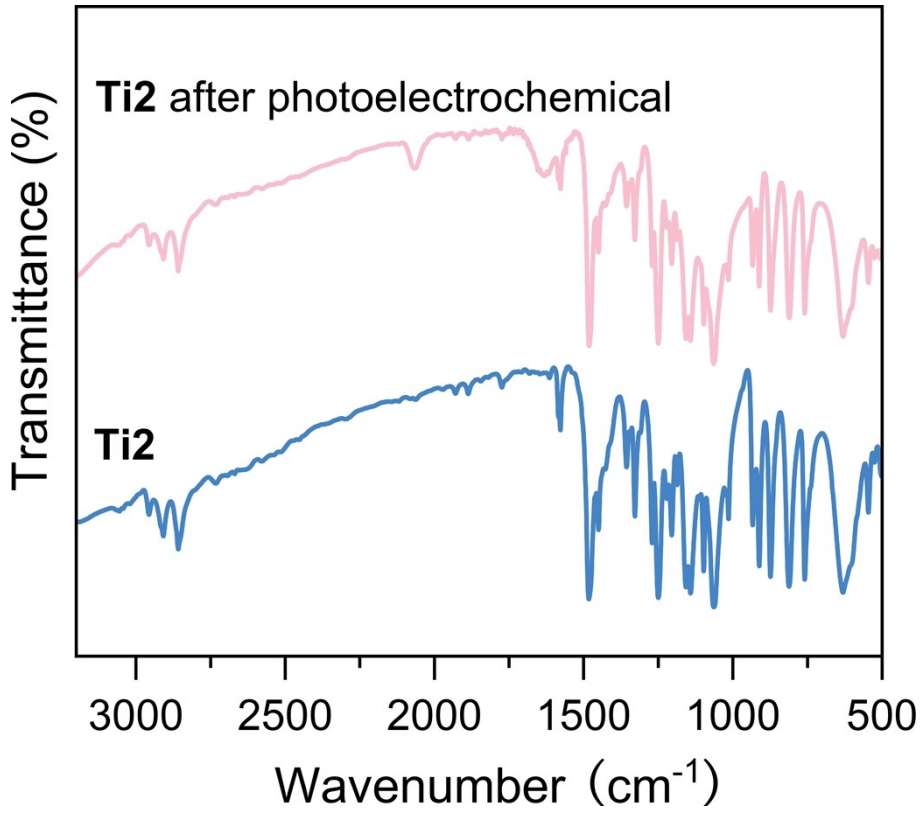

Figure S22. The IR spectra of the original crystals and the samples of **Ti8** after the photoelectrochemical test.

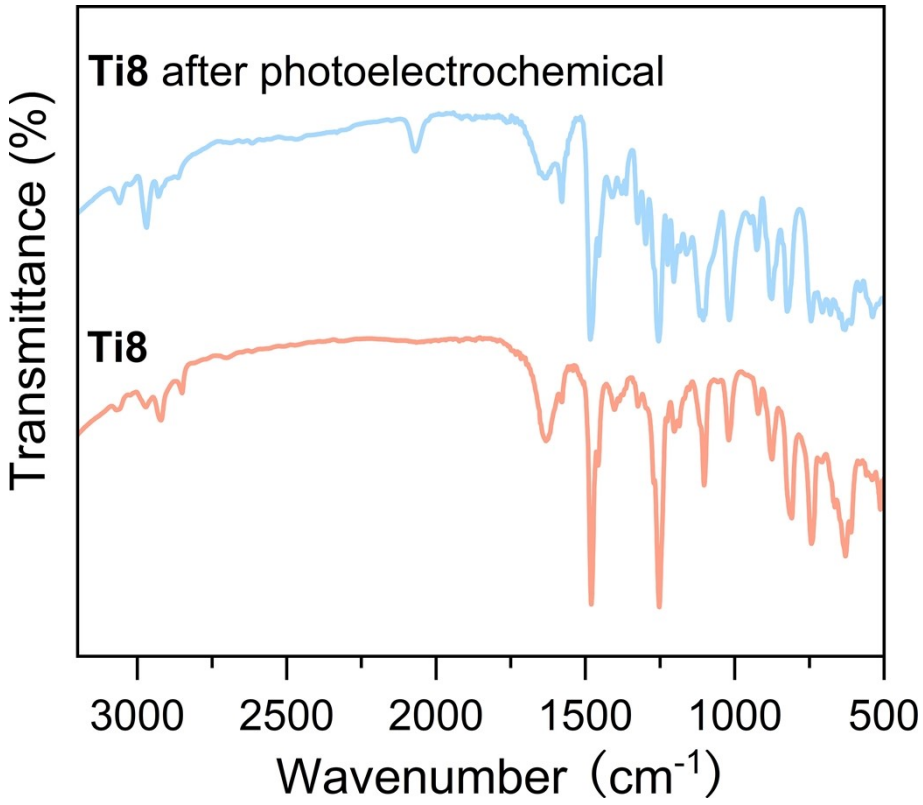

Figure S23. The IR spectra of the original crystals and the samples of **Ti16** after the photoelectrochemical test.

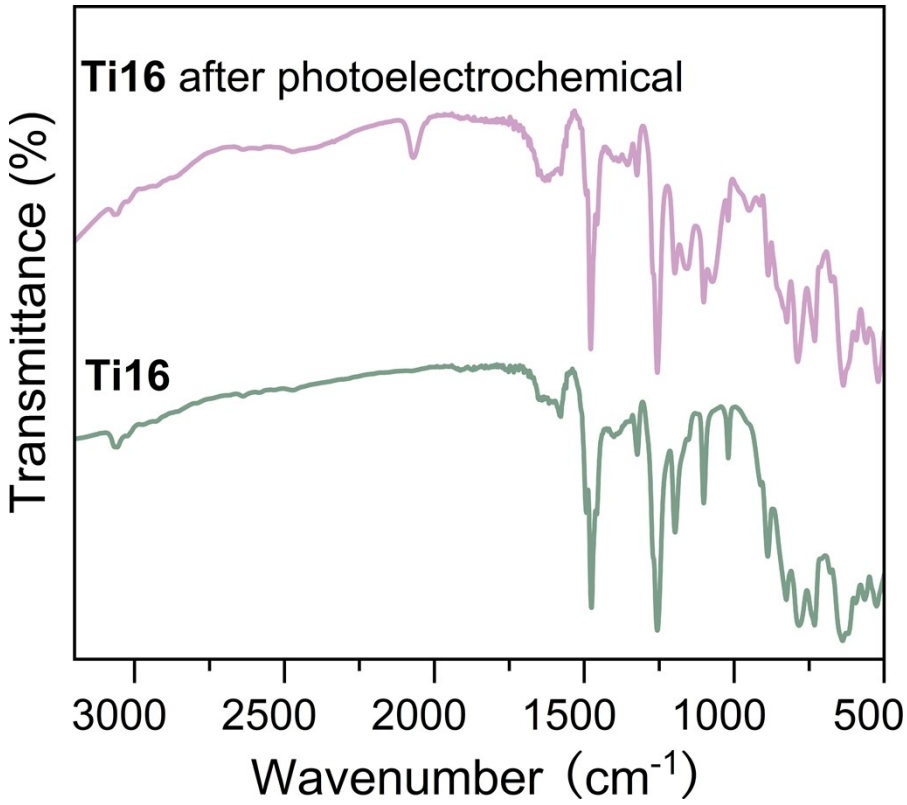

Figure S24. Isosurface plots (isodensity value = 0.02 a.u.) of molecular orbitals of (a) **Ti2** (b) **Ti8** and their corresponding energy levels.

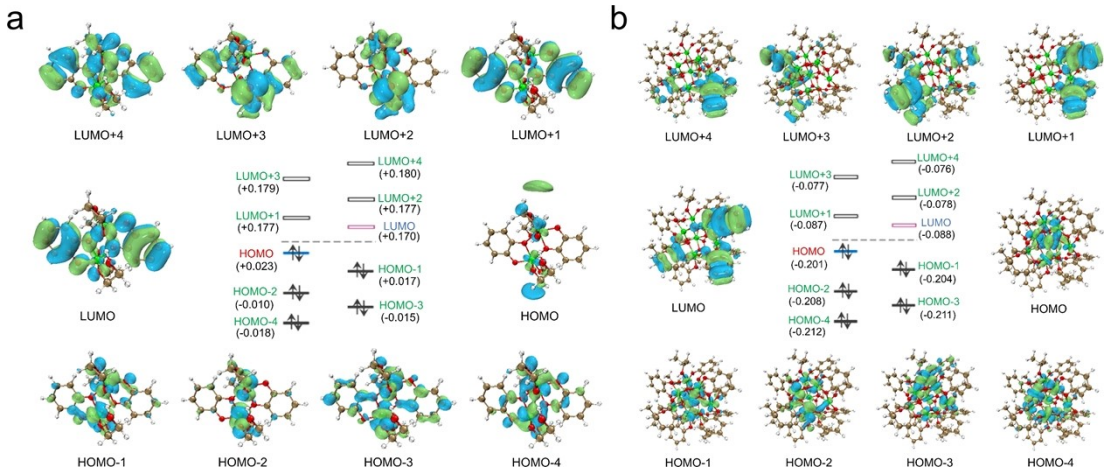

Table S1. Bond valence sum (BVS) analysis[g] for **Ti2**, **Ti8**, and **Ti16**.

Ti2		
Ti1 3.981		
Ti1–O1	d=2.087	0.449
Ti1–O1#1	d=2.0098	0.554
Ti1–O2	d=1.9474	0.655
Ti1–O3	d=2.178	0.351
Ti1–O4	d=1.833	0.893
Ti1–O6	d=1.763	1.079

Continued above

Ti8								
Ti1 3.999			**Ti2 3.794**			**Ti3 4.006**		
Ti1–O1	d=2.103	0.430	Ti2–O4	d=1.9808	0.599	Ti3–O13	d=2.158	0.371
Ti1–O2	d=1.942	0.665	Ti2–O15	d=2.0752	0.464	Ti3–O14	d=1.866	0.817
Ti1–O18	d=1.811	0.947	Ti2–O16	d=2.045	0.503	Ti3–O15	d=2.022	0.536
Ti1–O20	d=2.0067	0.558	Ti2–O19	d=1.9622	0.630	Ti3–O21	d=1.9451	0.659
Ti1–O21	d=2.0524	0.493	Ti2–O20	d=2.1237	0.407	Ti3–O24	d=2.066	0.476
Ti1–O23	d=1.828	0.905	Ti2–O21	d=2.054	0.491	Ti3–O25	d=1.74	1.148
			Ti2–O22	d=1.9227	0.701			
Ti4 3.777			**Ti5 3.845**			**Ti6 3.982**		
Ti4–O11	d=2.031	0.523	Ti5–O7	d=2.352	0.220	Ti6–O9	d=2.233	0.303
Ti4–O12	d=1.891	0.763	Ti5–O8	d=1.857	0.837	Ti6–O10	d=1.865	0.819
Ti4–O13	d=1.984	0.594	Ti5–O9	d=2.004	0.562	Ti6–O16	d=2.014	0.547
Ti4–O21	d=2.2558	0.285	Ti5–O11	d=2.065	0.477	Ti6–O19	d=1.9276	0.691
Ti4–O22	d=1.9536	0.644	Ti5–O22	d=1.9677	0.620	Ti6–O28	d=2.072	0.468
Ti4–O23	d=1.803	0.968	Ti5–O27	d=1.746	1.129	Ti6–O29	d=1.738	1.154
Ti7 3.945			**Ti8 3.959**					
Ti7–O5	d=2.088	0.448	Ti8–O1	d=1.958	0.637			
Ti7–O6	d=1.933	0.681	Ti8–O3	d=1.858	0.834			
Ti7–O7	d=1.9678	0.620	Ti8–O4	d=2.198	0.333			
Ti7–O17	d=1.81	0.950	Ti8–O5	d=1.976	0.607			
Ti7–O19	d=1.9472	0.656	Ti8–O20	d=2.1128	0.419			
Ti7–O20	d=1.9864	0.590	Ti8–O26	d=1.746	1.129			

Continued above

Ti16								
Ti1 3.889			**Ti2 3.829**			**Ti3 3.826**		
Ti1–O1	d=2.186	0.344	Ti2–O3	d=2.044	0.505	Ti3–O11	d=2.058	0.486
Ti1–O2	d=1.86	0.830	Ti2–O4	d=1.894	0.757	Ti3–O12	d=1.904	0.737
Ti1–O3	d=1.996	0.575	Ti2–O15	d=1.922	0.702	Ti3–O17	d=1.904	0.737
Ti1–O11	d=2.001	0.567	Ti2–O16	d=2.024	0.533	Ti3–O18	d=2.031	0.523
Ti1–O23	d=1.988	0.587	Ti2–O23	d=1.928	0.691	Ti3–O23	d=1.922	0.702
Ti1–O24	d=1.796	0.987	Ti2–O26	d=1.955	0.642	Ti3–O28	d=1.955	0.642
Ti4 3.890			**Ti5 3.820**			**Ti6 3.770**		
Ti4–O6	d=1.97	0.616	Ti5–O13	d=1.9	0.745	Ti6–O5	d=1.869	0.810
Ti4–O9	d=1.873	0.801	Ti5–O14	d=2.092	0.443	Ti6–O6	d=2.091	0.444
Ti4–O10	d=2.205	0.327	Ti5–O22	d=1.927	0.692	Ti6–O22	d=1.929	0.689
Ti4–O14	d=1.982	0.597	Ti5–O25$^{\#1}$	d=1.977	0.605	Ti6–O25	d=1.962	0.630
Ti4–O22	d=2.004	0.562	Ti5–O27$^{\#1}$	d=1.959	0.635	Ti6–O26	d=1.956	0.640
Ti4–O24	d=1.796	0.987	Ti5–O28	d=1.923	0.700	Ti6–O27	d=2.008	0.556
Ti7 3.942			**Ti8 3.981**					
Ti7–O7	d=2.233	0.303	Ti8–O18	d=2.009	0.555			
Ti7–O8	d=1.861	0.828	Ti8–O19	d=2.21	0.322			
Ti7–O16	d=2.007	0.558	Ti8–O20	d=1.854	0.843			
Ti7–O21	d=1.841	0.874	Ti8–O21	d=1.838	0.881			
Ti7–O25	d=1.9	0.745	Ti8–O27$^{\#1}$	d=1.883	0.780			
Ti7–O26	d=1.959	0.635	Ti8–O28	d=1.98	0.600			

[g] $V_i = \Sigma S_{ij} = \Sigma \exp[(r_1 - r_{ij})/B]$, where r_{ij} is the bond length between atoms i and j (with r_1 = 1.791 for Ti^{iv}-O). The constant B is referred to as the "universal parameter" and is approximately equal to 0.37 Å. S_{ij} is the valence of a bond between atoms i and j, and V_i is the sum of all bond valences of the bonds formed by a given atom.[1]

Table S2. A summary of catecholate functionalized TOCs (Ti > 3).

Formula	Number of catechol	Number of alkoxide group	Number of Ti atom	Refs.
$[Ti_4O_2(Cat)_4(PZ)_4(O^iPr)_4]$	4	4	4	[2]
$[Ti_6O(Cat)_6(O^iPr)_{10}]$	6	10	6	[3]
$[Ti_7O_4(O^iPr)_8(Cat)_5(FcCO_2)_2]$	5	8	7	[4]
$[Ti_7O_3(O^iPr)_{12}(Cat)_4(o\text{-}BDC)]$	4	12	7	[4]
$[Ti_8O_4(O^iPr)_{12}(O_3P\text{-}Phen)_4(Cat)_2]$	2	12	8	[5]
$[Ti_{10}O_6(O^nBu)_{12}(HO^nBu)_2(Cat)_8]$	8	14	10	[6]
$[Ti_{17}O_{24}(O^iPr)_{18}(Cat)_2]$	2	18	17	[7]
$[Ti_{17}O_{24}(Cat)_4(O^iPr)_{16}]$	4	16	17	[3]
$[Ti_{14}O_{12}(NBA)_{10}(Cat)_{10}(HCat)_2]$	12	none	14	[8]
$[Ti_{14}O_{11}(PA)_{10}(Cat)_{10}(HCat)_4]$	14	none	14	[8]
$[Ti_2(Cat)_2(OEgO)_2(OEgOH)_2]$	2	4	2	**This work**
$[Ti_8O_5(Cat)_9(O^iPr)_4(HO^iPr)_2]$	9	6	8	**This work**
$[Ti_{16}O_{16}(Cat)_{20}]$	20	none	16	**This work**

Abbreviations: H_2Cat = catechol; PZ = pyrazole; $FcCO_2$ = ferrocene-1-carboxylate; o-BDC = o-benzenedicarboxylate; HO^nBu = 1-Butanol; HNBA = n-butyric acid.

Table S3. Kinds of solid-state photothermal materials reported in the references.

Compound	Laser power ($W\ cm^{-2}$)	Heating rate ($^oC\ s^{-1}$)	Maximum temperature (^oC)	Irradiation distance (cm)	Ref.
Co-MOF	0.7	7.82	215.5	8	9
Ag NPs@MOF	0.7	13.2	239.8	8	10
La coordination polymer	2	9	145	/	11
Zr-PDI	0.7	14	160	/	12
DTC cocrystal	0.7	0.3	71.3	/	13
Zn-MOF	0.2	14	233	10	14
SD/Ag18a	0.9	8.2	187	20	15
Ag14	0.9	115	194	20	16
Ag43		55.3	141		
Ag48T	0.5	163	512	15	17
Ag48M		149	470		
Ti2	**0.6**	**89**	**249**	**15**	**This work**
Ti8		**98**	**310.9**		
Ti16		**126.5**	**317**		

Table S4. Crystal data collection and sructure refinement for **Ti2**, **Ti8**, **Ti16**, and **Ti16-Me**.

Compound	**Ti2**	**Ti8**
Empirical formula	$C_{20}H_{26}O_{12}Ti_2$	$C_{72}H_{79}O_{29}Ti_8$
Formula weight	554.21	1791.55
Temperature [K]	173.0	296.15
Crystal system	monoclinic	triclinic
Space group (number)	$P2_1/c$ (14)	$P\bar{1}$ (2)
a [Å]	9.0139(15)	13.7327(7)
b [Å]	14.186(2)	14.2235(7)
c [Å]	8.9545(14)	23.4194(12)
α [°]	90	87.685(2)
β [°]	90.487(7)	89.986(2)
γ [°]	90	66.441(2)
Volume [Å^3]	1145.0(3)	4189.1(4)
Z	2	2
ρ_{calc} [g/cm^3]	1.608	1.420
μ [mm^{-1}]	6.509	0.797
F(000)	572	1838
Radiation	CuK_α (λ = 1.54178 Å)	MoK_α (λ = 0.71073 Å)
2θ range [°]	11.63 to 133.12 (0.84 Å)	4.58 to 50.05 (0.84 Å)
Index ranges	−10 ≤ h ≤ 10 −16 ≤ k ≤ 16 −10 ≤ l ≤ 10	−16 ≤ h ≤ 16 −16 ≤ k ≤ 16 −27 ≤ l ≤ 27
Reflections collected	10855	180993
Independent reflections	2008 R_{int} = 0.0568 R_{sigma} = 0.0404	14774 R_{int} = 0.0562 R_{sigma} = 0.0230
Completeness to θ = 66.561°	99.5 %	99.9 %
Data / Restraints / Parameters	2008/0/154	14774/158/1026
Goodness-of-fit on F^2	1.092	1.046
Final R indexes [I≥2σ(I)]	R_1 = 0.0448 wR_2 = 0.1198	R_1 = 0.0414 wR_2 = 0.1073
Final R indexes [all data]	R_1 = 0.0472 wR_2 = 0.1218	R_1 = 0.0502 wR_2 = 0.1147
Largest peak/hole [e/Å^3]	0.71/-0.81	1.21/-0.91

Continued above

Compound	Ti16	Ti16-Me
Empirical formula	$C_{134}H_{100}O_{58}Ti_{16}$	$C_{154}H_{136}O_{56}Ti_{16}$
Formula weight	3404.53	3649.02
Temperature [K]	173.00	173.0
Crystal system	triclinic	triclinic
Space group (number)	$P\bar{1}$ (2)	$P\bar{1}$ (2)
a [Å]	15.114(4)	16.790(3)
b [Å]	16.444(5)	16.977(3)
c [Å]	17.284(5)	17.003(3)
α [°]	63.041(9)	113.206(7)
β [°]	64.513(13)	113.379(6)
γ [°]	71.596(9)	98.474(7)
Volume [Å^3]	3417.3(18)	3814.6(12)
Z	1	1
ρ_{calc} [gcm^{-3}]	1.654	1.588
μ [mm^{-1}]	8.315	7.481
F(000)	1720	1860
Radiation	CuK_α (λ = 1.54178 Å)	CuK_α (λ = 1.54178 Å)
2θ range [°]	6.10 to 134.14 (0.84 Å)	6.15 to 133.19 (0.84 Å)
Index ranges	−15 ≤ h ≤ 18 −17 ≤ k ≤ 19 0 ≤ l ≤ 20	−19 ≤ h ≤ 19 −20 ≤ k ≤ 20 −20 ≤ l ≤ 20
Reflections collected	11962	50385
Independent reflections	11962 R_{int} = 0.0836 R_{sigma} = 0.0894	13381 R_{int} = 0.0738 R_{sigma} = 0.0873
Completeness to θ = 67.072°	98.0 %	99.3 %
Data / Restraints / Parameters	11962/126/810	13381/106/897
Goodness-of-fit on F^2	1.050	1.039
Final *R* indexes [$I \geq 2\sigma(I)$]	R_1 = 0.0737 wR_2 = 0.1865	R_1 = 0.0894 wR_2 = 0.2563
Final *R* indexes [all data]	R_1 = 0.1185 wR_2 = 0.2212	R_1 = 0.1346 wR_2 = 0.2961
Largest peak/hole [e/Å^3]	1.52/-0.94	1.05/-0.64

Table S5. Selected bond lengths (Å) for **Ti2**.

Ti2	
Atom-Atom	**Length / Å**
Ti1–O1	2.087(2)
Ti1–O1$^{\#1}$	2.0098(18)
Ti1–O2	1.9474(19)
Ti1–O3	2.178(2)
Ti1–O4	1.833(2)
Ti1–O6	1.763(2)

Table S6. Selected bond lengths (Å) for **Ti8**.

Ti8			
Atom-Atom	**Length / Å**	**Atom-Atom**	**Length / Å**
Ti1–O1	2.103(2)	Ti5–O7	2.352(2)
Ti1–O2	1.942(2)	Ti5–O8	1.857(2)
Ti1–O18	1.811(2)	Ti5–O9	2.004(2)
Ti1–O20	2.0067(19)	Ti5–O11	2.065(2)
Ti1–O21	2.0524(19)	Ti5–O22	1.9677(19)
Ti1–O23	1.828(2)	Ti5–O27	1.746(2)
Ti2–O4	1.9808(19)	Ti6–O9	2.233(2)
Ti2–O15	2.0752(19)	Ti6–O10	1.865(2)
Ti2–O16	2.0450(19)	Ti6–O16	2.014(2)
Ti2–O19	1.9622(19)	Ti6–O19	1.9276(19)
Ti2–O20	2.1237(19)	Ti6–O28	2.072(2)
Ti2–O21	2.0540(19)	Ti6–O29	1.738(2)
Ti2–O22	1.9227(19)	Ti7–O5	2.088(2)
Ti3–O13	2.158(2)	Ti7–O6	1.933(2)
Ti3–O14	1.866(2)	Ti7–O7	1.9678(19)
Ti3–O15	2.022(2)	Ti7–O17	1.810(2)
Ti3–O21	1.9451(19)	Ti7–O19	1.9472(19)
Ti3–O24	2.066(2)	Ti7–O20	1.9864(19)
Ti3–O25	1.740(2)	Ti8–O1	1.958(2)
Ti4–O11	2.031(2)	Ti8–O3	1.858(2)
Ti4–O12	1.891(2)	Ti8–O4	2.198(2)
Ti4–O13	1.984(2)	Ti8–O5	1.976(2)
Ti4–O21	2.2558(19)	Ti8–O20	2.1128(19)
Ti4–O22	1.9536(19)	Ti8–O26	1.746(2)
Ti4–O23	1.803(2)		

Table S7. Selected bond lengths (Å) for **Ti16**.

Ti16			
Atom-Atom	**Length / Å**	**Atom-Atom**	**Length / Å**
Ti1–O1	2.186(6)	Ti5–O13	1.900(6)
Ti1–O2	1.860(6)	Ti5–O14	2.092(6)
Ti1–O3	1.996(6)	Ti5–O22	1.927(5)
Ti1–O11	2.001(6)	Ti5–O25$^{\#1}$	1.977(5)
Ti1–O23	1.988(5)	Ti5–O27$^{\#1}$	1.959(5)
Ti1–O24	1.796(6)	Ti5–O28	1.923(6)
Ti2–O3	2.044(6)	Ti6–O5	1.869(6)
Ti2–O4	1.894(6)	Ti6–O6	2.091(6)
Ti2–O15	1.922(6)	Ti6–O22	1.929(5)
Ti2–O16	2.024(6)	Ti6–O25	1.962(5)
Ti2–O23	1.928(6)	Ti6–O26	1.956(6)
Ti2–O26	1.955(5)	Ti6–O27	2.008(5)
Ti3–O11	2.058(6)	Ti7–O7	2.233(6)
Ti3–O12	1.904(7)	Ti7–O8	1.861(6)
Ti3–O17	1.904(6)	Ti7–O16	2.007(6)
Ti3–O18	2.031(6)	Ti7–O21	1.841(6)
Ti3–O23	1.922(6)	Ti7–O25	1.900(6)
Ti3–O28	1.955(6)	Ti7–O26	1.959(5)
Ti4–O6	1.970(6)	Ti8–O18	2.009(5)
Ti4–O9	1.873(6)	Ti8–O19	2.210(6)
Ti4–O10	2.205(6)	Ti8–O20	1.854(6)
Ti4–O14	1.982(6)	Ti8–O21	1.838(6)
Ti4–O22	2.004(5)	Ti8–O27$^{\#1}$	1.883(6)
Ti4–O24	1.796(6)	Ti8–O28	1.980(6)

Table S8. Selected bond lengths (Å) for **Ti16-Me**.

Ti16-Me			
Atom-Atom	**Length / Å**	**Atom-Atom**	**Length / Å**
Ti1–O25	1.929(4)	Ti5–O26	1.938(5)
Ti1–O26	1.934(5)	Ti5–O10	2.013(5)
Ti1–O27	1.972(5)	Ti5–O6	2.023(5)
Ti1–O1	2.116(5)	Ti5–O9	1.891(5)
Ti1–O23$^{\#1}$	1.970(4)	Ti5–O24	1.917(5)
Ti1–O2	1.859(5)	Ti5–O5	1.938(5)
Ti2–O25	1.974(5)	Ti6–O26	1.965(5)
Ti2–O1	1.969(5)	Ti6–O27	1.892(4)
Ti2–O20	1.967(5)	Ti6–O28	1.840(5)
Ti2–O21	1.821(5)	Ti6–O8	1.855(5)
Ti2–O3	2.196(5)	Ti6–O10	2.023(5)
Ti2–O4	1.859(5)	Ti6–O7	2.267(5)
Ti3–O25	1.951(5)	Ti7–O22	1.961(5)
Ti3–O22	1.931(5)	Ti7–O14	2.021(5)
Ti3–O27$^{\#1}$	1.978(4)	Ti7–O15	2.034(5)
Ti3–O19	1.866(5)	Ti7–O24	1.929(5)
Ti3–O20	2.103(5)	Ti7–O16	1.904(5)
Ti3–O23	1.983(5)	Ti7–O13	1.900(5)
Ti4–O15	1.987(6)	Ti8–O22	1.960(5)
Ti4–O21	1.787(5)	Ti8–O23	1.891(4)
Ti4–O6	2.012(5)	Ti8–O18	1.856(5)
Ti4–O24	1.950(5)	Ti8–O28	1.852(5)
Ti4–O11	2.282(7)	Ti8–O14	2.025(5)
Ti4–O12	1.833(6)	Ti8–O17	2.271(5)

Reference

1 I. D. Brown, Recent Developments in the Methods and Applications of the Bond Valence Model, *Chem. Rev.*, 2009, **109**, 6858-6919.

2 X. Fan, H. Fu, L. Zhang, J. Zhang and X. Fan, Pyrazole-thermal synthesis: a new approach towards N-rich titanium-oxo clusters with photochromic behaviors, *Dalton Trans.*, 2019, **48**, 8049-8052.

3 J. B. Benedict and P. Coppens, The Crystalline Nanocluster Phase as a Medium for Structural and Spectroscopic Studies of Light Absorption of Photosensitizer Dyes on Semiconductor Surfaces, *J. Am. Chem. Soc.*, 2010, **132**, 2938-2944.

4 J.-L. Hou, P. Huo, Z.-Z. Tang, L.-N. Cui, Q.-Y. Zhu and J. Dai, A Titanium Oxo Cluster Model Study of Synergistic Effect of Co-coordinated Dye Ligands on Photocurrent Responses, *Inorg. Chem.*, 2018, **57**, 7420-7427.

5 H.-T. Lv, H.-M. Li, G.-D. Zou, Y. Cui, Y. Huang, Y. Fan and H.-T. Lv, Titanium-oxo clusters functionalized with catecholate-type ligands: modulating the optical properties through charge-transfer transitions, *Dalton Trans.*, 2018, **47**, 8158-8163.

6 K. Gigant, A. Rammal and M. Henry, Synthesis and Molecular Structures of Some New Titanium(IV) Aryloxides, *J. Am. Chem. Soc.*, 2001, **123**, 11632-11637.

7 C. Liu, J. Hu, F. Zhu, J. Zhan, L. Du, C. H. Tung and Y. Wang, Functionalization of Titanium Oxide Cluster $Ti_{17}O_{24}(OC_3H_7)_{20}$ with Catechols: Structures and Ligand-Exchange Reactivities, *Chem. Eur. J.*, 2019, **25**, 14843-14849.

8 M.-Y. Gao, Z. Wang, Q.-H. Li, D. Li, Y. Sun, Y. H. Andaloussi, C. Ma, C. Deng, J. Zhang and L. Zhang, Black Titanium-Oxo Clusters with Ultralow Band Gaps and Enhanced Nonlinear Optical Performance, *J. Am. Chem. Soc.*, 2022, **144**, 8153-8161.

9 T. Yan, Y. Y. Li, J. Su, H. Y. Wang and J. L. Zuo, Charge Transfer Metal-Organic Framework Containing Redox-Active TTF/NDI Units for Highly Efficient Near-Infrared Photothermal Conversion, *Chem. Eur. J.*, 2021, **27**, 11050-11055.

10 J. Su, P. Cai, T. Yan, Z.-M. Yang, S. Yuan, J.-L. Zuo, H.-C. Zhou and J. Su, Enhancing the photothermal conversion of tetrathiafulvalene-based MOFs by redox doping and plasmon resonance, *Chem. Sci.*, 2022, **13**, 1657-1664.

11 S. Wang, S. Li, J. Xiong, Z. Lin, W. Wei, Y. Xu and S. Wang, Near-infrared photothermal conversion of stable radicals photoinduced from a viologen-based coordination polymer, *Chem. Commun.*, 2020, **56**, 7399-7402.

12 B. Lü, Y. Chen, P. Li, B. Wang, K. Müllen and M. Yin, Stable radical anions generated from a porous perylenediimide metal-organic framework for boosting near-infrared photothermal conversion, *Nat. Commun.*, 2019, **10**, 767.

13 Y. Wang, W. Zhu, W. Du, X. Liu, X. Zhang, H. Dong and W. Hu, Cocrystals Strategy towards Materials for Near-Infrared Photothermal Conversion and Imaging, *Angew. Chem., Int. Ed.,* 2018, **130**, 4027-4031.

14 Q. Gu, Z.-H. Zhao, B. Chan, T. Yan, J.-L. Zuo, D. M. D'Alessandro and C.-H. Li, Efficient Photothermal Energy Conversion Triggered by near-Infrared Light in a Dithiolene-Based Metal–Organic Framework, *ACS Materials Lett.,* 2023, **5**, 603-607.

15 Z. Wang, L. Li, L. Feng, Z.-Y. Gao, C.-H. Tung, L.-S. Zheng and D. Sun, Solvent-Controlled Condensation of $[Mo_2O_5(PTC4A)_2]^{6-}$ Metalloligand in Stepwise Assembly of Hexagonal and Rectangular Ag18 Nanoclusters, *Angew. Chem., Int. Ed.*, 2022, **134**, e202200823.

16 Z. Wang, Y.-J. Zhu, B.-L. Han, Y.-Z. Li, C.-H. Tung and D. Sun, A route to metalloligands consolidated silver nanoclusters by grafting thiacalix[4]arene onto polyoxovanadates, *Nat. Commun.*, 2023, **14**, 5295.

17 K. Sheng, Z. Wang, L. Li, Z.-Y. Gao, C.-H. Tung and D. Sun, Solvent-Mediated Separation and Reversible Transformation of 1D Supramolecular Polymorphs Built from $[W_{10}O_{32}]^{4-}$ Templated 48-Nuclei Silver(I) Cluster, *J. Am. Chem. Soc.*, 2023, **145**, 10595-10603.